Supplementary materials:

Hollow sphere structured V_2O_3@C as an anode material for high capacity potassium-ion batteries

Fei Chen, Shuo Wang, Xiao-Dong He, Jia-Ying Liao, Qiao Hu, Jie-Min Dong, Chun-Hua Chen *

CAS Key Laboratory of Materials for Energy Conversions, Department of Materials Science and Engineering & Collaborative Innovation Center of Suzhou Nano Science and Technology, University of Science and Technology of China, Anhui Hefei 230026, China

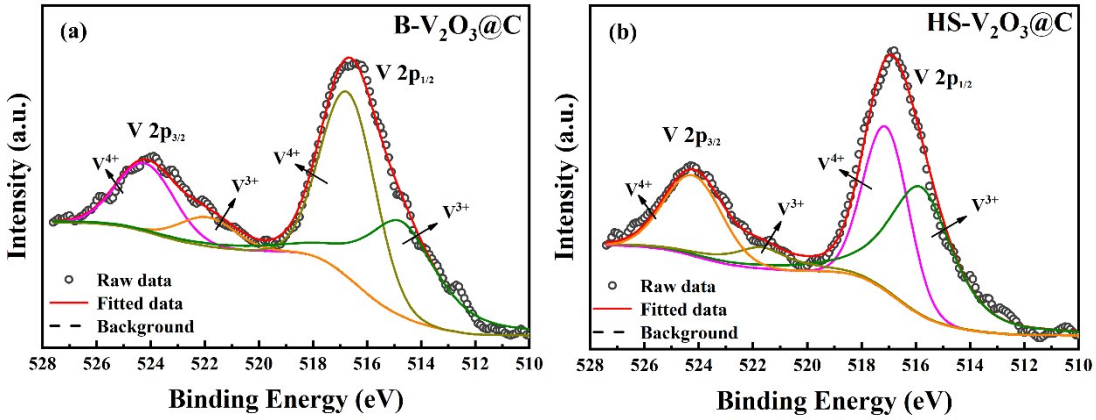

Figure S1. High-resolution XPS spectrum of V 2p of B-V_2O_3@C (a) and HS-V_2O_3@C materials (b).

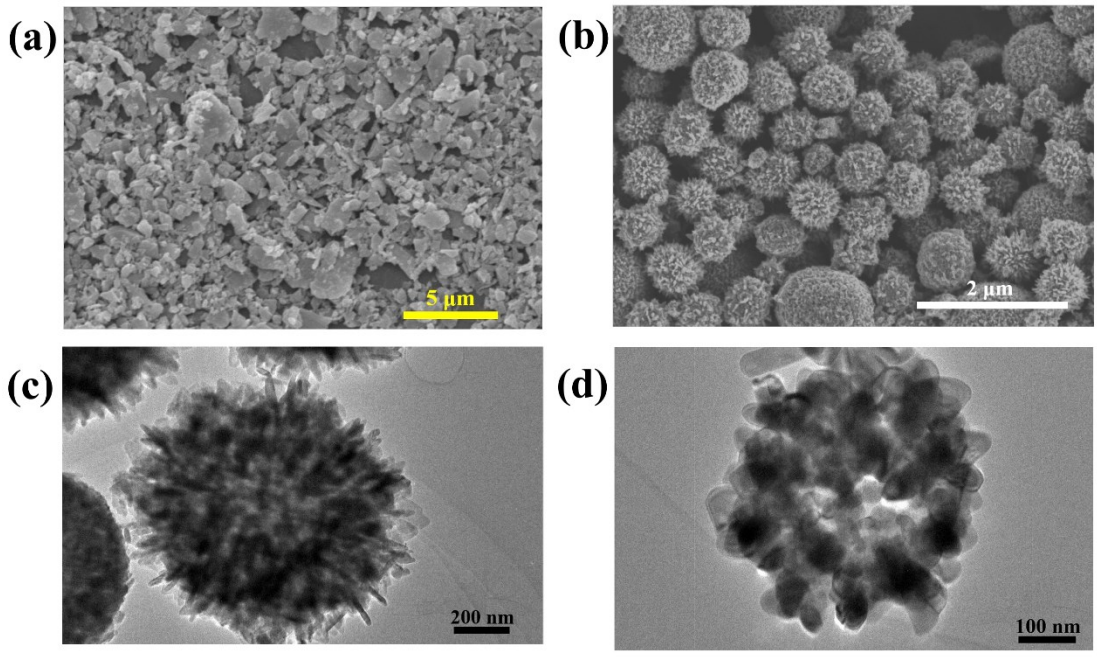

Figure S2. SEM images of B-V_2O_3@C (a) and HS-VO_2 (b); TEM images of HS-VO_2 (c) and HS-V_2O_3 (d).

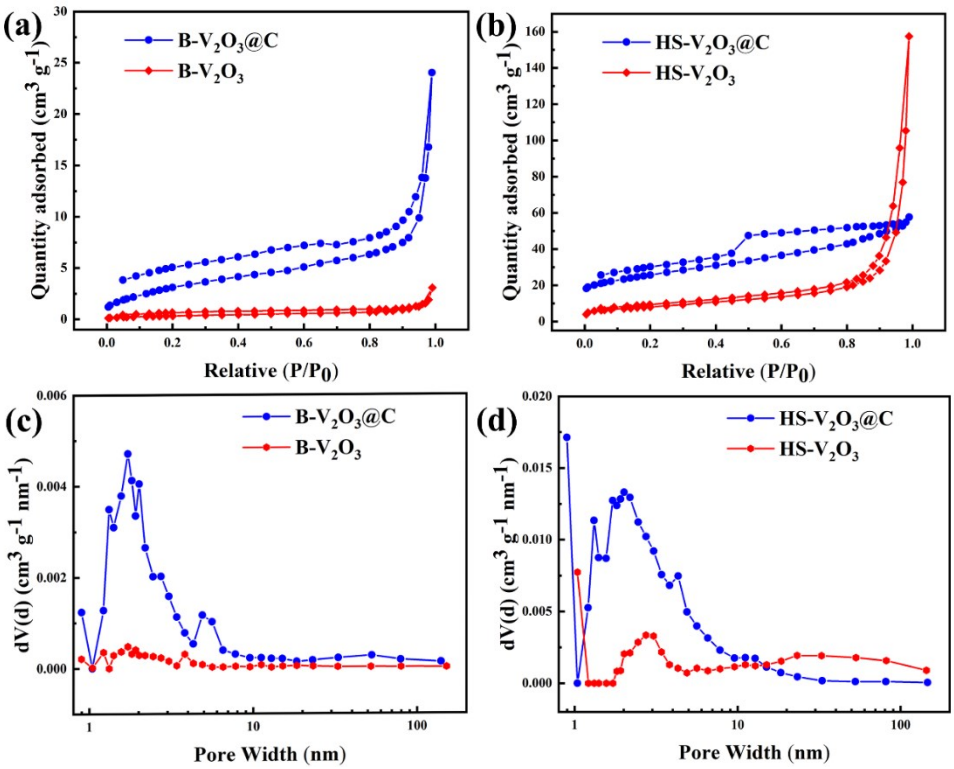

Figure S3. Nitrogen adsorption-desorption isotherms and the pore size distributions of bulk V_2O_3 (a, c) and hollow sphere V_2O_3 (b, d).

Table S1. Electronic conductivity of HS-V_2O_3@C and HS-V_2O_3 samples

Sample	Electronic conductivity (S cm^{-1})
HS-V_2O_3@C	9.011 x 10^{-3}
HS-V_2O_3	3.397 x 10^{-3}

In order to verify that the carbon coating layer can improve the electronic conductive property of materials, we have measured the electronic conductivity of HS-V_2O_3@C and HS-V_2O_3 samples through a four-probe method. Testing electrodes were prepared by mixing active materials and PVDF with the ratio of 8:1. The obtained slurry was cast onto an insulating substrate and dried in vacuum at 70°C for 12 h to remove excess solvent and cut to Φ10 mm sheets. The calculation results show that through the carbon coating method, the electronic conductivities of HS-V_2O_3 enhance from 3.397 x 10^{-3} S cm^{-1} to 9.011 x 10^{-3} S cm^{-1}, indicating that carbon coating can effectively improve the electron transmission ability of V_2O_3.

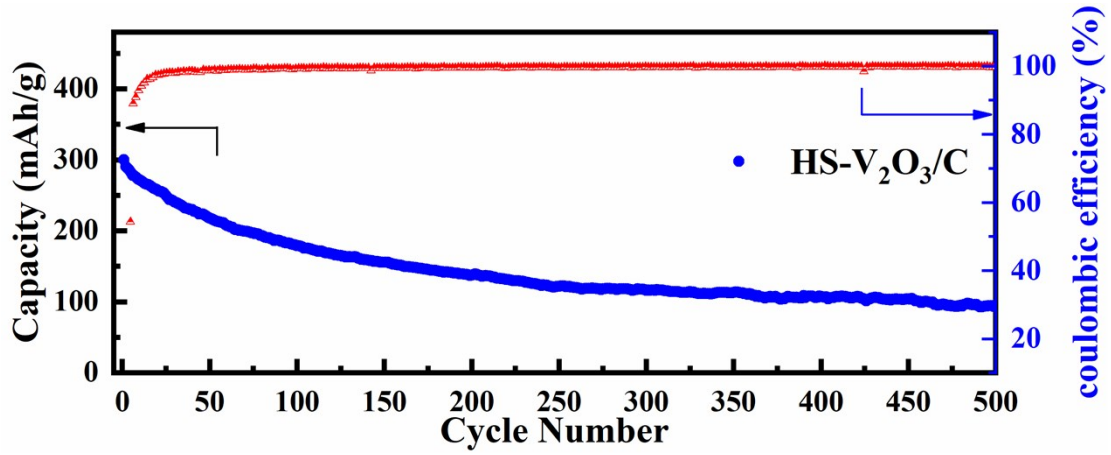

Figure S4. Cycle performance for HS-V_2O_3/C electrode at 100 mA g^{-1}.

Table S2. The concentration of vanadium dissolved into electrolyte after 100 cycles examined by ICP analysis.

Sample	Concentration of V (μg ml^{-1})
HS-V_2O_3@C	0.178
HS-V_2O_3/C	0.357

For the sake of verifying the dissolution of vanadium element with low valence state into electrolyte, we prepared the HS-V_2O_3/C sample (by mixing HS-V_2O_3 and carbon reduced from PVA in a mortar, the final carbon content is 30.0 wt%) and evaluated its cycle performance. The capacity decay is very serious, after 500 cycles, only 90 mA h g^{-1} left.

We disassembled the half-cells after 100 cycles under an argon atmosphere in glove box, took out the electrode films, and they were immersed in 2 ml of DME solvent for one month. However, there is no significant color difference can be observed between the HS-V_2O_3-@C material and the HS-V_2O_3/C material. This may because only a trace of vanadium element is dissolved in the DME. In order to compare the dissolution content of the vanadium element in the two solutions, we performed an ICP analysis. We firstly took out the electrode films, evaporated the DME solvent at 120°C, and then completely dissolved the residue with an equal volume (2 ml) of concentrated nitric acid. According to the analysis results of ICP, the dissolution phenomenon of the HS-V_2O_3/C sample into electrolyte is more serious. For the HS-V_2O_3/C sample, in which the surface of V_2O_3 has no coating layer, bare V_2O_3 particles can contact with electrolyte directly. It is more likely to cause the dissolution of low valence state

transition metal ions. And the carbon coating layer of the HS-V_2O_3-@C material is very uniform, can suppress the dissolution of vanadium effectively.

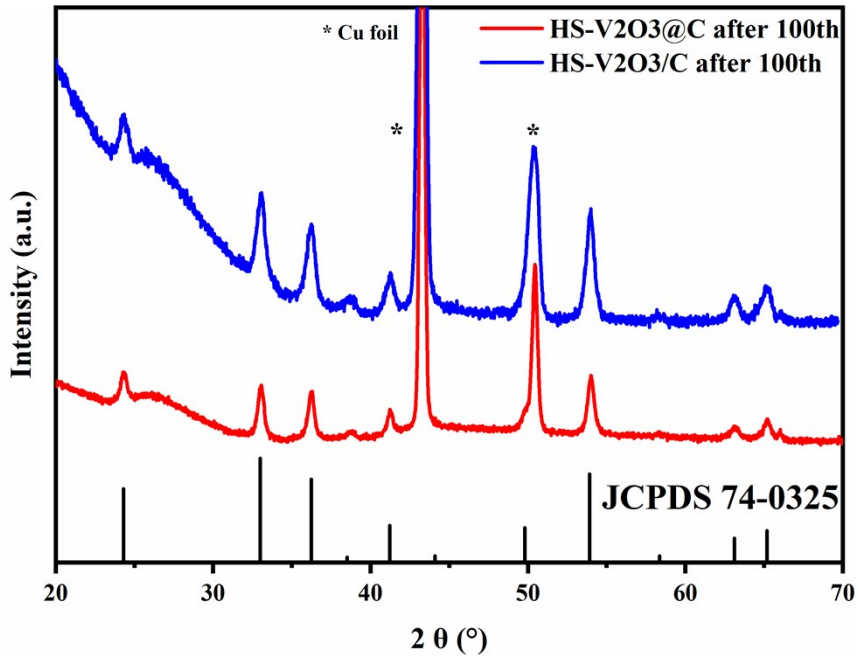

Figure S5. The *ex situ* XRD patterns of HS-V_2O_3@C and HS-V_2O_3/C electrodes after 100 cycles (current density: 200 mA g^{-1}).

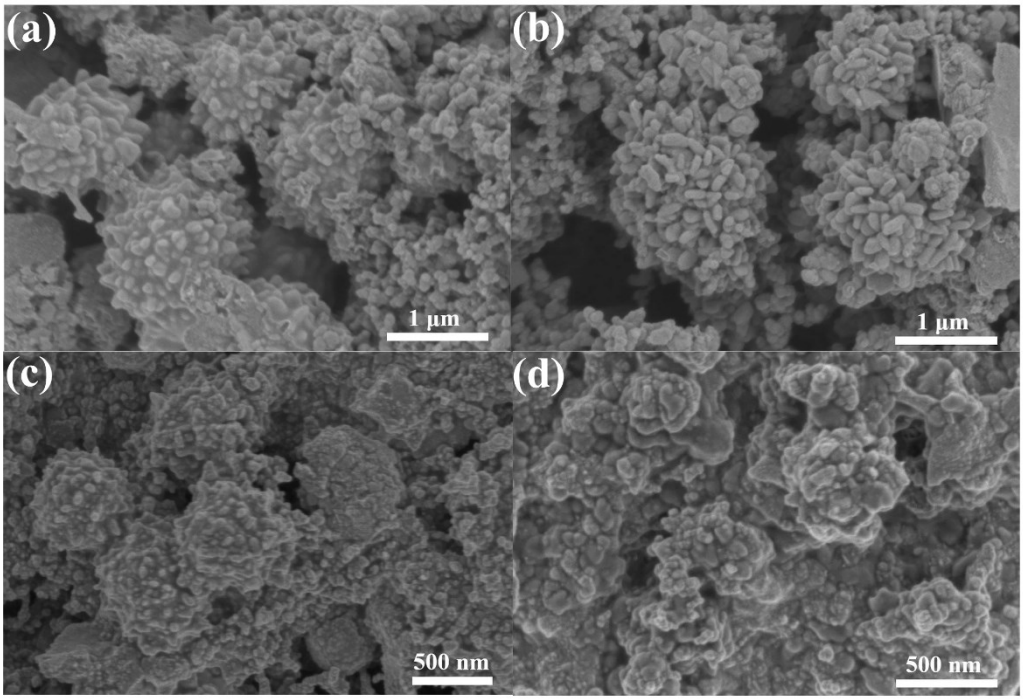

Figure S6. SEM images of HS-V_2O_3@C before (a) and after (c) 100 cycles (current density: 200 mA g^{-1}); HS-V_2O_3/C before (b) and after (d) 100 cycles (current density:

200 mA g^{-1}).

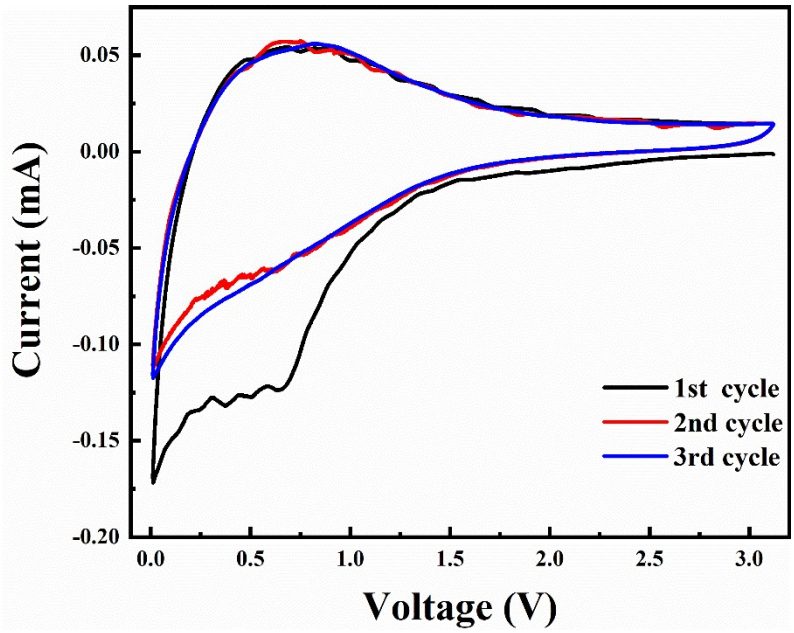

Figure S7. The initial 3 cycles of CV curves of HS-V_2O_3@C electrode at 0.1 mV s^{-1}.

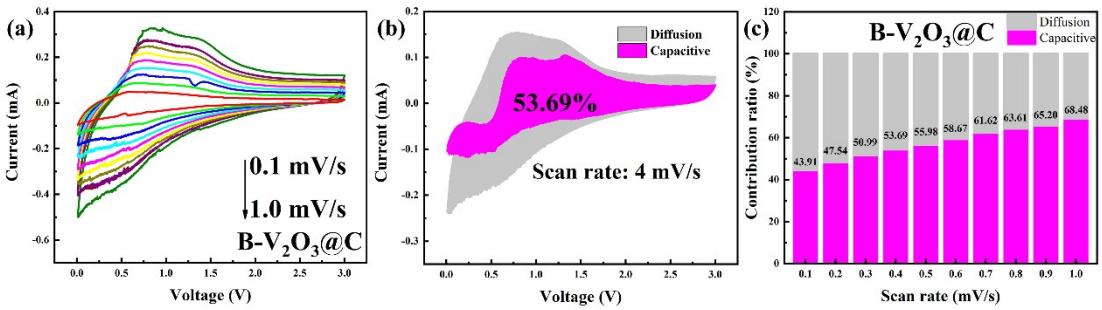

Figure S8. Electrochemical analyses of B-V_2O_3@C electrodes: (a) CV curves of B-V_2O_3@C electrode at different scan rates; The contribution percentages from capacitive and diffusion effect of B-V_2O_3@C electrode at 4 mV/s (b) and other scan rates (c).

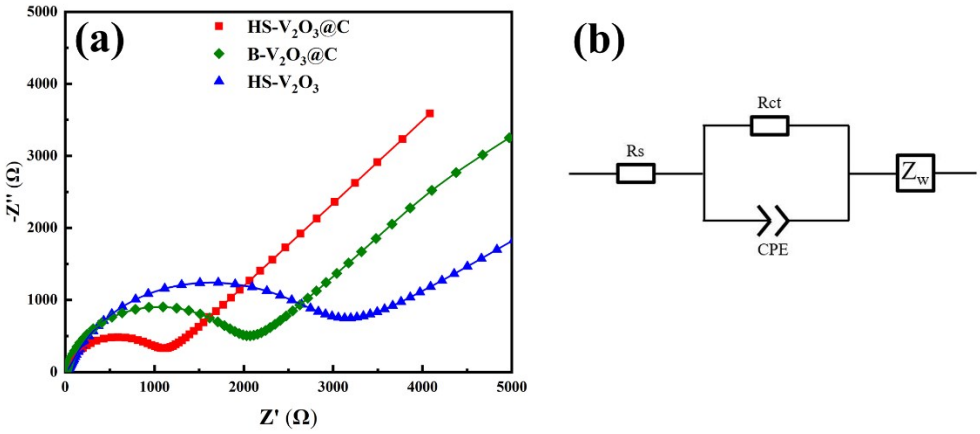

Figure S9. (a) EIS spectra of HS-V_2O_3@C, B-V_2O_3@C and HS-V_2O_3 samples; (b) the equivalent circuit used for the experimental impedance data.

Table S3. The fitted impedances of HS-V_2O_3@C, B-V_2O_3@C and HS-V_2O_3.

sample	Rs (Ω)	Rct (Ω)
HS-V_2O_3@C	7.471	961.7
B-V_2O_3@C	7.194	1806.0
HS-V_2O_3	7.825	2538.0

We performed the EIS results of HS-V_2O_3@C, HS-V_2O_3 and B-V_2O_3@C samples to compare the electron and ion transport properties. The EIS spectra are fitted using the equivalent circuit model (Fig. S9b), where Rs represents solution resistance corresponding to the electrolyte and electrical contacts, and Rct represents charge-transfer resistance for the electrons and K^+. For all of the samples, the value of Rs is approximately equal, while the HS-V_2O_3@C possess the lowest Rct values, which is in good agreement of its superior rate performance and cycling stability. Compared with B-V_2O_3@C, HS-V_2O_3 has the highest Rct value even with a smaller particle size, proving that carbon coating effectively decreases the charge-transfer resistance.

Table S4. Comparison of recent reported intercalation anode materials for PIBs.

Sample	Electrolyte	Capacity Retention	Rate Capability	Reference
Hard carbon	0.8 M KPF_6 / EC:DEC	155 mA h g^{-1} / 200 cycles at 0.5C	60 mA h g^{-1} at 2C	S1
Soft carbon	0.8 M KPF_6 / EC:DEC	160 mA h g^{-1} / 50 cycles at 2C	140 mA h g^{-1} at 5C	S2
WS_2	5 M KTFSI / DEGDME	60 mA h g^{-1} / 600 cycles at 20 mA g^{-1}	30 mA h g^{-1} at 500 mA g^{-1}	S3
Hard-Soft composite carbon	0.8 M KPF_6 / EC:DEC	186 mA h g^{-1} / 200 cycles at 1C	121 mA h g^{-1} at 10C	S4
York-Shell carbon sphere	0.8 M KPF_6 / EC:DEC	138 mA h g^{-1} / 1200 cycles at 200 mA g^{-1}	121 mA h g^{-1} at 5000 mA g^{-1}	S5
$K_2Ti_8O_{17}$	0.8 M KPF_6 / EC:DEC	110.7 mA h g^{-1} / 50 cycles at 20 mA g^{-1}	44.2 mA h g^{-1} at 500 mA g^{-1}	S6
HS-V_2O_3@C	3 M KFSI / DME	330 mA h g^{-1} / 500 cycles at 100 mA g^{-1}	79 mA h g^{-1} at 5000 mA g^{-1}	This work

Reference

S1. Y.C. Li, R.A. Adams, A. Arora, V.G Pol, A.M. Levine, R.J. Lee, K. Akato, A.K. Naskar and M.P. Paranthaman, *J. Electrochem. Soc.*, 2017, **164**, A1234-A1238.

S2. Z.L. Jian, W. Luo and X.L. Ji, *J. Am. Chem. Soc.*, 2015, **137**, 11566-11569.

S3. R. Zhang, J. Bao, Y. Pan and C.F. Sun, *Chemical Science*, 2019, **10**, 2604-2612.

S4. Z.L. Jian, S. Hwang, Z.F. Li, A.S. Hernandez, X.F. Wang, Z. Y. Xing, D. Su and X.L. Ji, *Adv. Funct. Mater.*, 2017, **27**, 1700324.

S5. H. Zhang, H. He, J. Luan, X. Huang, Y. Tang and H. Wang, *J. Mater. Chem. A*, 2018, **6**, 23318-23325.

S6. J. Han, M.W. Xu, Y.B. Niu, G.N. Li, M.Q. Wang, Y. Zhang, M. Jia and C.M. Li, *Chem. Commun.*, 2016, **52**, 11274-11276.